Saturation spectroscopy with laser optical pumping in atomic barium

P. G. Pappas, M. M. Burns, D. D. Hinshelwood, and M. S. Feld
Department of Physics and Spectroscopy Laboratory, Massachusetts Institute of Technology, Cambridge, Massachusetts 02139

D. E. Murnick
Bell Laboratories, Murray Hill, New Jersey 07974

(Received 2 March 1979; revised manuscript received 24 January 1980)

The magnitude and sign of laser saturation resonances induced in atomic transitions with level degeneracy can be dramatically altered by the presence of optical pumping. This paper presents a detailed theoretical treatment of optical-pumping Lamb dips and crossover resonances, and their experimental observation in the 553-nm barium resonance transition. The physical principles underlying the laser optical-pumping saturation effect are also discussed.

I. INTRODUCTION

Over the past decade saturation spectroscopy has provided a powerful tool for attaining narrow "Doppler-free" resonances in molecular systems.[1] This has led to a wealth of information about spectroscopic structure and line-broadening mechanisms. Now, with the availability of tunable single-mode dye lasers, these techniques can be extended to a wide variety of atomic resonance transitions. However, when studying saturation effects (Lamb dips, crossover resonances, laser-induced line-narrowing effects, etc.) in such systems a new class of features arises. Atomic systems set themselves apart in that at low pressures the relaxation of the excited state is dominated by radiative decay to the ground state, thus forming an isolated two-level system in which the number of atoms is conserved. As is well known, optical-pumping effects can occur in atomic systems of this kind.[2] The presence of optical pumping and the ensuing induced atomic orientation can lead to saturation effects with unusual properties, for example, anomalous intensities of various spectral features. In fact, under appropriate conditions a reversal in sign of saturation resonances can occur. By studying this type of behavior one can obtain quantitative information about the effectiveness and details of the optical-pumping process in the system under study. In addition, the ability to induce selective atomic (and in some cases nuclear) orientation over a narrow portion of the atomic velocity distribution has important potential applications.[3] This paper presents a simple theoretical description of this effect and experimental results in atomic barium.[4] Some recent related work is presented in Refs. 5, 6, and 7.

The techniques of laser saturation spectroscopy are based on the selective saturation induced by an intense beam of monochromatic laser radiation interacting with a Doppler-broadened transition. As an example, consider a Lamb-dip-type[8] experiment performed on an initially unexcited two-level system, center frequency ω, in which the sample is simultaneously subjected to two monochromatic beams of the same frequency Ω, an intense beam, and a weak counterpropagating probe beam [Fig. 1(a)]. Owing to saturation, the intense field pumps atoms in the lower level into the upper level. However, not all atoms interact, only those in the narrow portion of the velocity distribution which is Doppler shifted into resonance [Fig. 1(b)]. These narrow changes manifest themselves as a resonant increase in the transmission of the probe field as it is tuned through the center of the Doppler profile ($\Omega = \omega$).

The presence of optical pumping can strongly enhance the saturation effect. Optical pumping[2] gives rise to a net transfer of atoms to higher or lower orientation quantum number, depending on the polarization of the applied field. If the field is right circularly polarized, for example, the selection rule for absorption is $\Delta M = +1$, whereas for spontaneous reemission $\Delta M = 0, \pm 1$ is generally allowed. Hence the pumping cycle tends to shift the population to higher M levels, leading to a selective buildup of population in specific ground

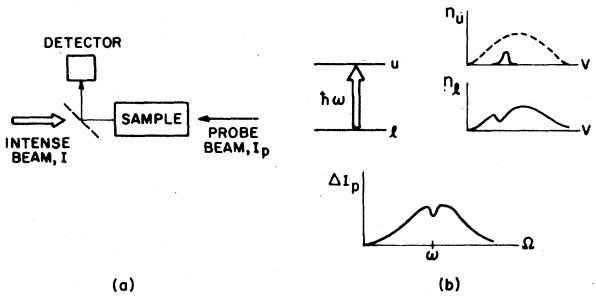

FIG. 1. Lamb-dip effect. (a) Experimental scheme. (b) Energy levels, velocity distributions, and probe absorption ΔI_p.

and excited M states. The degree of orientation depends on the atomic transition, as well as the extent of relaxation and transit time effects. Effective optical pumping does not require a laser field. In fact, optical-pumping studies using conventional broadband light sources were carried out many years before the advent of lasers.[9]

A Lamb-dip experiment of the type described above can be influenced by optical pumping in several ways. For simplicity, consider the case in which the intense beam is right circularly polarized and the transition is of the $J=1-0$ type, with the population equally distributed among the M states of the $J=1$ ground state in the absence of the laser field (Fig. 2). According to the above selection rules, the saturating field induces transitions between the $M=+1$ lower level and the upper ($J=M=0$) level, and hence pumps atoms in a narrow velocity band from this lower level into the upper level. However, the excited-state atoms undergo radiative decay to lower states $M=0$ and -1, as well as to the $M=+1$ state where they originated. Accordingly, in the course of the optical-pumping cycle atoms in the narrow velocity band are removed from the $M=+1$ lower level and accumulate in the $M=0$ and $M=-1$ levels [Figs. 2(b) and 2(c)]. Thus, when the Lamb-dip tuning condition $\Omega=\omega$ is satisfied, a reflected counterpropagating probe beam will sense an unusually large depletion of ground-state atoms, hence an abnormally deep Lamb dip [Fig. 2(b)]. On the other hand, a linearly polarized probe beam (or a probe beam of the opposite circular polarization) will sense a buildup of ground-state population, hence a reversal in sign of the Lamb dip [Fig. 2(c)]. Similar behavior can occur in crossover resonances,[10] in saturation resonances in three-level systems[11] (such as coupled fine-structure transitions), and in many other types of saturation spectroscopy experiments in which strong optical pumping occurs.

The above example assumes *complete* optical pumping, hence neglects the influence of cross-relaxation processes. In any realistic system nonradiative relaxation effects will tend to destroy the orientation developed in the optical-pumping process. Even if collisional effects are negligible (as in the experiments described below), the extent of the optical pumping will be limited by the finite duration of the light-atom interaction, determined by the transit time of the atoms as they traverse the pump beam. The balance reached between optical pumping and relaxation gives rise to a steady-state population distribution with a given degree of orientation. A theoretical formulation of the laser optical-pumping saturation effect is given in the next section.

The remainder of this paper is divided into three sections. Section II presents a theoretical formulation of the laser optical-pumping saturation resonances: Section II A describes the physical principles involved; Sec. II B formulates the laser optical-pumping saturation effect; and Sec. II C calculates the line shapes of optical-pumping Lamb dip and crossover resonances in systems with simple level structure. Section III discusses the laser optical-pumping saturation effect as observed in atomic barium. Section III A presents the experimental information and Sec. III B describes the extension of the theory to the barium system, where the effects of level degeneracy become important. Some concluding remarks are given in Sec. IV.

II. THEORY

A. Physical principles

As mentioned in the Introduction, the balance reached between laser optical pumping and relaxation gives rise to a steady-state population

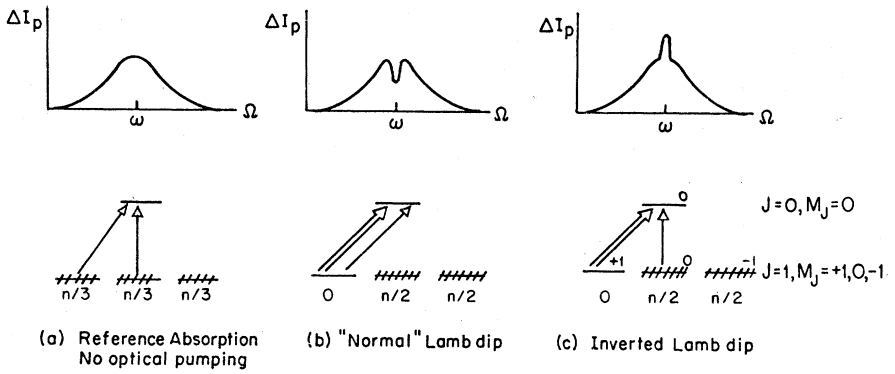

FIG. 2. Optical-pumping Lamb dip. Double arrows: saturating beam; single arrows: probe beam. (b) Saturating beam is rhc polarized; probe beam is lhc polarized. (c) Saturating beam is rhc polarized; probe beam is linearly polarized.

distribution with a given degree of orientation. This steady-state condition can be formulated naturally in terms of a saturation process in which the usual saturation parameter I_s is reduced by a factor $\sim T/\tau$, where τ is the radiative lifetime and T is the effective lifetime of the ground state, which is not "stable" due to effects such as collisional relaxation and transit time. For example, at sufficiently low pressures where the transit time limits the atom-field interaction time, $T \sim d/u$, with d the diameter of the pump beam and u the average atomic velocity. Since typically T is in the μ sec range and $\tau \simeq 10$ nsec, this reduction factor can be sizable. Accordingly, large saturation effects can be achieved at relatively small pump intensities. Similarly, the dependence of the saturation parameter on transit time makes it possible to control experimentally the degree of optical pumping by varying the diameter of the laser beam.

To understand how the effective ground-state lifetime influences the saturation process, consider the simplified energy level scheme of Fig. 3, a Doppler-broadened three-level system in which two degenerate or near-degenerate M states 1 and 2 are optically coupled to a common upper M state 0 by electric dipole transitions. A monochromatic pump field interacts with the 2-0 transition. Level 0 can decay via spontaneous emission to levels 1 and 2 with rates Γ_1 and Γ_2, respectively, resulting in a radiative lifetime $\tau = 1/(\Gamma_1 + \Gamma_2)$. Thus, after absorbing a pump photon at the $2 \rightarrow 0$ transition, the atom can either return to state 2, with probability $\Gamma_2\tau$, or decay to state 1, with probability $\Gamma_1\tau$. Accordingly, the applied field will cause atoms initially in level 2 to accumulate in level 1. In particular, in the case of a short-lived excited state with large branching ($\Gamma_1 \gg \Gamma_2$) the probability of transferring an atom from levels 2 to 1 in an interaction time t is given by

$$P_{2\rightarrow 1} = \mathcal{A}t = (\sigma_0 I/\hbar\omega)t\,, \tag{1}$$

where $\mathcal{A}$ is the probability/sec of an atom in level 2 making a transition to level 1, $\hbar\omega$ is the photon energy, σ_0 is the 2-0 absorption cross section, and I the intensity of the pump field. However,

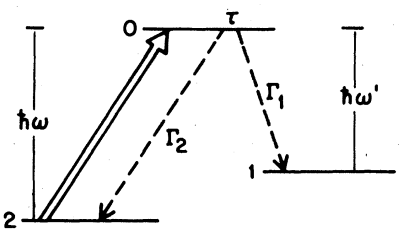

FIG. 3. Optical-pumping saturation effect, simplified energy level diagram.

this process cannot continue indefinitely, since the atom can only interact with the beam for a duration T. Thus, an atom initially in state 2 will have a large probability of being transferred to state 1 when

$$(\sigma_0 I/\hbar\omega)T = 1\,, \tag{2}$$

i.e., when the intensity of the laser field satisfies the condition

$$I \equiv I' = \hbar\omega/\sigma_0 T\,. \tag{3}$$

Hence, if T is large a substantial fraction of the population of level 2 can be transferred to level 1, even for relatively small values of I. Put another way, optical pumping can lead to an effective decrease of the usual saturation intensity parameter[12]

$$I_s = \hbar\omega/2\sigma_0\tau \tag{4}$$

to a value I', smaller than I_s by a factor $2\tau/T \ll 1$.

B. Laser optical-pumping saturation effect

Consider the three-level system of Fig. 3, in which $2 \rightarrow 0$ is the absorbing transition and $1 \rightarrow 0$ the branching transition. The applied field only resonates with the $2 \rightarrow 0$ transition, whose homogeneously broadened absorption cross section is of the form

$$\sigma(x) = \sigma_0 \frac{(\gamma/2)^2}{(\Delta - x)^2 + (\gamma/2)^2}\,, \tag{5}$$

with σ_0 the peak value of σ, $\Delta = \Omega - \omega$ the detuning of the intense field from the $2 \rightarrow 0$ atomic center frequency, and $x = kv$ the frequency shift due to atomic motion, $k = \omega/c$, v = velocity component along the propagation direction z of the saturating field. γ, the homogeneous linewidth (FWHM), is given by

$$\gamma = 1/\tau + 2/T\,. \tag{6}$$

Notice that T contributes to γ, since nonradiative relaxation (collisions, transit time, etc.) decreases the effective lifetime of each level and thus increases the linewidth of the transition. As usual,

$$\sigma_0 = 8\pi k\mu^2/\hbar\gamma\,, \tag{7}$$

with μ the electric dipole matrix element of the $2 \rightarrow 0$ transition.

The growth of the applied field intensity I is determined by the equation

$$dI/dz = \alpha I\,, \tag{8}$$

where α is the velocity integrated gain coefficient:

$$\alpha = \int (n_0 - n_2)\sigma(x)dx\,, \tag{9}$$

with $n_j(v)dv$ the population density of level j for the velocity group of atoms in the narrow interval between v and $v+dv$. The level population equations are

$$\dot{n}_2 = (n_0 - n_2)(\sigma I/\hbar\omega) + n_0\Gamma_2 + (n_2^0 - n_2)/T\,, \tag{10a}$$

$$\dot{n}_0 = -(n_0 - n_2)(\sigma I/\hbar\omega) - n_0(1/\tau + 1/T)\,, \tag{10b}$$

$$\dot{n}_1 = n_0\Gamma_1 + (n_1^0 - n_1)/T\,. \tag{10c}$$

Here n_1^0 and n_2^0 are the steady-state population densities of levels 1 and 2 for a particular velocity group when $I=0$ (it is assumed that $n_0^0=0$):

$$n_j^0 = N_j G(x)\,, \tag{11a}$$

with N_j the total population density of level j and $G(x)$ the normalized velocity distribution

$$\int_{-\infty}^{\infty} G(x)dx = 1\,. \tag{11b}$$

Number conservation requires that

$$n_0 + n_1 + n_2 = n_1^0 + n_2^0\,. \tag{12}$$

Nonradiative relaxation is included through the terms $(n_j^0 - n_j)/T$, where n_j^0/T is a source term denoting the rate at which atoms in state j are produced, and n_j/T is the rate at which they relax. (See Sec. IV for further discussion.) The condition $n_j=0$, $I=0$ then fixes n_j^0 as the background density of level j. Note then Eqs. (10) and (12) give

$$\dot{n}_0 + \dot{n}_1 + \dot{n}_2 = 0 \tag{13}$$

as they should.

The steady-state solution to Eqs. (10), obtained for $\dot{n}_j=0$, is straightforward:

$$n_2 = n_2^0\left[1 - \frac{I}{I+I_1}\left(\frac{1+\Gamma_1 T}{2+\Gamma_1 T}\right)L(x)\right]\,, \tag{14a}$$

$$n_0 = n_2^0\frac{I}{I+I_1}\left(\frac{1}{2+\Gamma_1 T}\right)L(x)\,, \tag{14b}$$

$$n_1 = n_1^0 + n_2^0\frac{I}{I+I_1}\left(\frac{\Gamma_1 T}{2+\Gamma_1 T}\right)L(x)\,, \tag{14c}$$

with $L(x)$ the power-broadened line-shape factor,

$$L(x) = \frac{(\gamma/2)^2(1+I/I_1)}{(\Delta - x)^2 + (\gamma/2)^2(1+I/I_1)}\,, \tag{15}$$

and I_1 the laser optical-pumping saturation intensity parameter,

$$I_1 = \frac{\hbar\omega}{\sigma_0\tau}\left(\frac{1+\tau/T}{2+\Gamma_1 T}\right). \tag{16}$$

The gain coefficient, Eq. (9), is then

$$\alpha = -N_2\int_{-\infty}^{\infty}\left(1 - \frac{I}{I+I_1}L(x)\right)\sigma(x)G(x)dx\,, \tag{17}$$

where Eq. (11a) has been used. In Doppler-broadened atomic systems the Doppler width ku is several GHz, much broader than the homogeneous width γ which is typically of the order of several MHz. Therefore, in the expression for α the velocity distribution $G(x)$ is slowly varying compared to γ, and so may be removed from the integrand and evaluated at $x=\Delta$. The remaining integral is straightforward, giving

$$\alpha = \frac{-N_2\sigma_D(\Delta)}{(1+I/I_1)^{1/2}}\,, \tag{18}$$

with $\sigma_D(\Delta)$ the usual Doppler-broadened absorption cross section[13]:

$$\sigma_D(\Delta) = \tfrac{1}{2}\pi\gamma\sigma_0 G(\Delta) = (4\pi^2 k\mu^2/\hbar)G(\Delta)\,. \tag{19}$$

Equation (18) is the same as the usual gain coefficient expression Eq. (9) except that the usual saturation parameter I_s, Eq. (4), is replaced by I_1, the laser optical-pumping saturation parameter.

It is clear from Eq. (16) that laser optical pumping causes saturation effects to set in at a lower intensity than would otherwise be expected. Let us inspect some limiting cases of I_1. For no branching $\Gamma_1 T \to 0$ and

$$I_1 \to I_\infty = (\hbar\omega/2\sigma_0\tau)(1+\tau/T)\,. \tag{20}$$

Equation (20) is only the same as the "usual" saturation parameter I_s, Eq. (4), for $T \gg \tau$. This shows that even in the absence of optical pumping, nonradiative relaxation can be important, and that in general (20) must be used rather than (4). The presence of branching always reduces I_1 from I_∞, as can be seen from the ratio ($\Gamma_1 \gg \Gamma_2$),

$$I_1/I_\infty = (2+\Gamma_1 T)^{-1}\,. \tag{21}$$

An important case is the limit of large branching ($\Gamma_1 \gg \Gamma_2$), $\Gamma_1\tau \to 1$, a situation occurring when the excited state 0 can decay to several lower states, so that radiative decay can proceed through many channels. In this case

$$I_1 \to \frac{\hbar\omega}{\sigma_0 T}\left(\frac{1+\tau/T}{1+2\tau/T}\right). \tag{22}$$

Thus, for $T \gg \tau$

$$I_1 \to I' = \hbar\omega/\sigma_0 T\,, \tag{23}$$

as anticipated in Eq. (3).

C. Optical-pumping laser saturation resonances

1. *Optical-pumping lamb dips*

Now consider the transmission of a weak counterpropagating probe field, also at frequency Ω, simultaneously interacting with the atomic system. For the present, levels 2 and 1 will be considered to be degenerate M states (i.e., $\omega=\omega'$ in Fig. 3).

First assume that the polarization of the probe field is such that it interacts only with the 2-0 transition. In this case the probe field gain coefficient, defined in the same manner as in Eq. (8), is given by[14]

$$\alpha_p = \int (n_0 - n_2)\sigma(-x)dx\,, \tag{24}$$

the sign of x, the Doppler shift, being reversed from Eq. (9) because the probe field is a counterpropagating wave. Thus, the expression for α_p is the same as in Eq. (17), except that $\sigma(x)$ is replaced by $\sigma(-x)$ [cf. Eq. (5)]. Integration in the Doppler limit then yields

$$\alpha_p = -N_2\sigma_D(\Delta)\left(1 - S\frac{(w/2)^2}{\Delta^2 + (w/2)^2}\right), \tag{25}$$

with saturation factor S describing the depth of the resonance,

$$S = \frac{I/I_1}{(1+I/I_1)^{1/2}[1+(1+I/I_1)^{1/2}]}, \tag{26}$$

and

$$w = \tfrac{1}{2}\gamma[1+(1+I/I_1)^{1/2}]. \tag{27}$$

The first term in Eq. (25) is the usual linear attenuation of the weak probe beam. The second term gives the change signal induced by the intense field, a Lorentzian of width (FWHM) w. This change signal is of the same form as the usual Lamb-dip expression,[8] except that I_s is replaced by I_1. Thus, for a given pump intensity I a deeper and wider Lamb dip will occur than that obtained in the absence of optical pumping.

Finally, note that in the above discussion it was not necessary to assume that levels 2 and 1 are degenerate. Thus, Eq. (25) for α_p also describes a Lamb-dip resonance in a two-level system ($2 \rightarrow 0$ transition) with a coupled branching transition at $\omega' \neq \omega$. For example, in the barium system $2 \rightarrow 0$ would be the ^1P-^1S resonance transition ($\lambda = 553$ nm) and $1 \rightarrow 0$ the ^1P-^1D branching transition (λ 1.50 μm).

Next, consider a Lamb-dip experiment in a transition with degenerate M states in which the polarization of the probe beam is such that it resonates only with the $1 \rightarrow 0$ transition. In this case the probe gain coefficient is given by

$$\alpha_p = \int (n_0 - n_1)\sigma'(-x)dx\,, \tag{28}$$

where $\sigma'(-x)$, the absorption cross section of the $1 \rightarrow 0$ transition, is of the same form as Eq. (5) except that σ_0 is replaced by σ_0', the $1 \rightarrow 0$ peak absorption cross section. Using Eqs. (14) and (11), integration in the Doppler limit yields

$$\alpha_p = \sigma_D'(\Delta)\left[-N_1 + N_2\left(\frac{1-\Gamma_1 T}{2+\Gamma_1 T}\right)S\frac{(w/2)^2}{\Delta^2 + (w/2)^2}\right], \tag{29}$$

with $\sigma_D'(\Delta)$ the $1 \rightarrow 0$ Doppler-broadened absorption cross section. This change signal expression is the same as in Eq. (25) except for the additional factor $(1-\Gamma_1 T)/(2+\Gamma_1 T)$, due to population transfer from level 2 to level 1 via optical pumping. For $\Gamma_1 T \ll 1$ (i.e., partial lifetime of the $1 \rightarrow 0$ branching transition is much longer than the nonradiative relaxation time) the behavior of the narrow resonance is the same as in the previous case. (The $\frac{1}{2}$ reduction factor is due to the fact that only level 0, and not level 2, contributes to the resonant behavior in this case.) For nonzero values of $\Gamma_1 T$, however, its behavior changes. As $\Gamma_1 T \rightarrow 1$ its amplitude reduces to zero, and for $\Gamma_1 T > 1$ it undergoes a sign change, becoming equal (but of opposite sign) to the case of Eq. (25) for $\Gamma_1 T \gg 1$.[17] The physical origin of this sign change, the transfer of population from level 2 to level 1, was discussed in Sec. I.

2. *Optical-pumping crossover resonance*

Similar behavior can also manifest itself in laser-induced crossover resonances.[10] In this type of saturation experiment the configuration is the same as in a Lamb-dip experiment except that the Doppler profiles of the $2 \rightarrow 0$ and $1 \rightarrow 0$ coupled transitions do not coincide, but partially overlap ($\gamma < |\omega - \omega'| < ku$, Fig. 3), as might occur in a transition with hyperfine structure. (For level structure of this type the selection rules are usually such that pump and probe fields can both couple to the $1 \rightarrow 0$ and $2 \rightarrow 0$ transitions.) In this case an additional narrow resonant change signal occurs when the applied fields are tuned exactly midway between the two resonances: $\Omega = \frac{1}{2}(\omega + \omega')$. This new change signal comes about because the saturating field can resonate with the $2 \rightarrow 0$ and $1 \rightarrow 0$ Doppler profiles simultaneously, inducing atomic transitions into level 0 in two velocity bands centered at v_1 and v_2, determined by the tuning conditions for the $2 \rightarrow 0$ and $1 \rightarrow 0$ resonances, respectively,

$$\Omega - \omega = kv_2\,, \tag{30a}$$

$$\Omega - \omega' = kv_1\,. \tag{30b}$$

The counterpropagating probe field can interact with these atoms when they are Doppler shifted into resonance:

$$\Omega + (kv_1 \text{ or } kv_2) = \omega\,, \tag{31a}$$

$$\Omega + (kv_1 \text{ or } kv_2) = \omega'\,. \tag{31b}$$

Inserting Eqs. (30) into (31) gives the three solutions, $\Omega = \omega$ ($2 \rightarrow 0$ Lamb dip), $\Omega = \omega'$ ($1 \rightarrow 0$ Lamb

dip), and $\Omega = \frac{1}{2}(\omega + \omega')$, the crossover resonance condition.

The calculation of the crossover resonances change signals is similar to the previous ones. In this case $\omega' \neq \omega$ and so the 1-0 absorption cross section is of the form

$$\sigma_1(-x) = \sigma_0' \frac{(\gamma/2)^2}{(\Delta' + x)^2 + (\gamma/2)^2}, \tag{32}$$

with $\Delta' = \Omega - \omega'$ the detuning of the probe field from the 1-0 atomic center frequency. The part of α_p containing the crossover resonances is then given by

$$\alpha_p = \int (n_0 - n_1)\sigma_1(-x)dx + \mathfrak{K}, \tag{33}$$

where $\mathfrak{K}$ is an identical term but with Δ and Δ', subscripts 1 and 2, and σ_0' and σ_0 interchanged everywhere (neglecting interference terms which are unimportant when $|\omega - \omega'| \gg \gamma$). The first term of (33) describes the interaction of the pump field resonating at the $2 \rightarrow 0$ transition with the probe field resonating at the $1 \rightarrow 0$ transition and the second term describes the reverse interaction. Substituting Eqs. (14) and (32) into (33), and integrating in the Doppler limit then gives

$$\alpha_p = \sigma_D'(\Delta')\left[-N_1 + N_2\left(\frac{1-\Gamma_1 T}{2+\Gamma_1 T}\right) S \frac{(w/2)^2}{(\Omega-\omega_c)^2 + (w/2)^2}\right] + \sigma_D(\Delta)\left[-N_2 + N_1\left(\frac{1-\Gamma_2 T}{2+\Gamma_2 T}\right) S' \frac{(w'/2)^2}{(\Omega-\omega_c)^2 + (w'/2)^2}\right], \tag{34}$$

where ω_c is the center frequency of the crossover resonance,

$$\omega_c = \tfrac{1}{2}(\omega + \omega'), \tag{35}$$

and S', w', and I_2 are defined in the same way as S, w, and I_1, respectively, except for replacing subscript 1 with 2. The behavior of this change signal is very similar to that of the Lamb dip on a coupled transition, as can be seen by comparing Eqs. (34) and (29). Hence, abnormally deep saturation signals of either sign can occur.

Crossover resonances with reversed sign have been reported by Hänsch, Shahin, and Schawlow.[18] A calculation of this effect has been given by Holt.[19]

III. APPLICATION TO ATOMIC BARIUM

A. Experimental

Optical-pumping laser saturation dips were studied on the resonance transition of atomic barium, a $^1P_1 \rightarrow {}^1S_0$ transition at $\lambda = 553.5$ nm. The $^1P_1$ upper level can radiatively decay to the $^1D_2$ metastable state ($\lambda = 1.50\ \mu$m), as well as to the

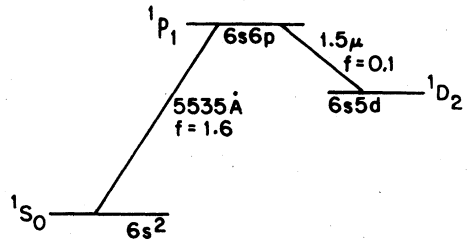

FIG. 4. Barium level scheme.

$^1S_0$ ground state (Fig. 4). The lifetime of the upper level is 8.4 nsec, with a 4% branching ratio to the $^1D_2$ state.

Natural barium has five common isotopes. Their resonance transitions are closely spaced and their Doppler profiles all overlap. The odd isotopes have nuclear spins of $I = \frac{3}{2}$, and so the P state is split into three hyperfine levels with $F = \frac{5}{2}, \frac{3}{2}$, and $\frac{1}{2}$. The hyperfine structure and isotope splittings of the resonance transitions are not resolvable by ordinary means, but have been studied by Jackson and Tuan[20] and Rasmussen, Schieder, and Walther[21] using atomic beams. The isotopic abundances and isotope and hyperfine transition center frequencies are listed in Table I.

The experiments used a single-mode cw dye laser with Rhodamine 110 dye, pumped by a 4-W argon ion laser. The dye laser produced up to 150 mW of single-mode radiation tunable over 30 GHz, with a linewidth of approximately 1 MHz. A 25-mg sample of isotopically naturally abundant barium was placed in a cell, which in turn was placed inside a temperature-controlled oven and then connected to a pumping station. This setup allowed simultaneous heating and pumping of the

TABLE I. Isotopic abundances and $\lambda = 553$-nm isotope and hyperfine transition center frequencies in naturally occurring barium.

Isotope	% abundance	Hyperfine components (F upper)	Relative frequency (MHz) [a]
138	72		0
137	11	$\frac{5}{2}$	65
		$\frac{3}{2}$	260
		$\frac{1}{2}$	555
136	8		125
135	6.6	$\frac{5}{2}$	105
		$\frac{3}{2}$	305
		$\frac{1}{2}$	535
134	2.4		140

[a] From Refs. 20 and 21.

cell, and hence cell pressure could be constantly monitored. The cell was a pyrex cylinder 1 in. in diameter and 1 in. long with $\lambda/10$ optical windows. The windows on the oven were $\lambda/10$ fused silica optical flats, and the oven heating coils were carefully counterwound to eliminate stray magnetic fields during heating. Optimal oven temperatures were in the 450–500 °C range, hot enough to produce vapor, but cool enough to prevent blackening of the cell windows. At these temperatures the cell pressure was maintained at $\approx 8 \times 10^{-7}$ Torr by an ion pump.

The experimental setup is depicted in Fig. 5. The dye-laser output was split into two parts, an intense saturating beam and a weaker, counter-propagating probe beam. The diameters of both beams at the cell were adjusted to 1.25 mm by use of a telescope and irises. The two beams overlapped in the sample cell. The probe beam, which was slightly misaligned, passed by the knife edge of a mirror which reflected the saturating beam into the sample cell and was directed onto a detector photomultiplier (Fig. 5). To suppress the Doppler background and improve the signal-to-noise ratio the saturating beam was chopped at 2 kHz and the probe beam absorption was lock-in detected. The polarization and intensity of each beam could be independently varied using quarter-wave and half-wave plates, linear polarizers, and neutral density filters. For the data shown in Fig. 6, the pump and probe powers were 45 and 5 μW, respectively. Under these conditions the magnitude of the saturation resonances was approximately 0.7% of that of the Doppler background.

Figure 6 shows experimental traces of the saturation resonances taken with two different polarization configurations, illustrating some of the effects described in Sec. II. The expected spectrum is complicated, being composed of 15 components, each of width $\simeq$20 MHz (FWHM), which all fall within the Doppler profile: (i) nine Lamb dips, one for each of the three even isotopes and three for each of the odd isotopes, which occur at the atomic center of each isotopic hyperfine component, and (ii) six crossover resonances, three for each odd isotope. These fall midway between hyperfine component pairs $\frac{1}{2}$-$\frac{3}{2}$, $\frac{1}{2}$-$\frac{5}{2}$, and $\frac{3}{2}$-$\frac{5}{2}$, where each hyperfine component is designated by the F quantum number of its upper level. (The lower levels are all $F=\frac{3}{2}$.) The calculations discussed in the next section predict that nine of these saturation components are prominent, the other six being small and unresolved. The identity of the components are labeled in Fig. 6. The most striking features are (1) the simultaneous occurence of saturation resonances of opposite signs [e.g., (a) and (l)]; (2) the change in sign of resonance (n) with polarization configuration; (3) the fact that crossover resonance (l) is inverted and of comparable intensity to the ^{138}Ba Lamb dip (a), which would be expected to be eight times more intense based on relative abundances and statistical weights alone. These unusual features are all manifestations of the optical-pumping laser saturation effect. The observed linewidths are about 26 MHz (FWHM), the additional 6 MHz of broadening being due to laser linewidth (1 MHz), power broadening (2.5 MHz), and misalignment

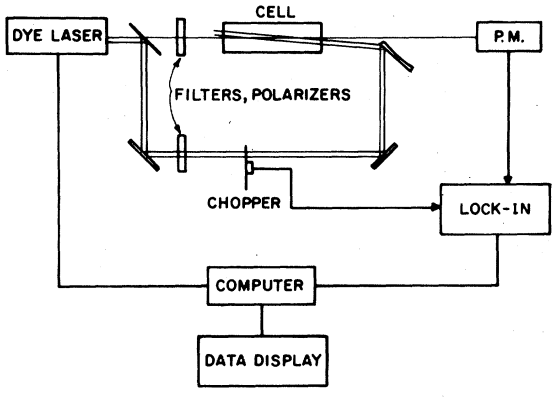

FIG. 5. Experimental setup.

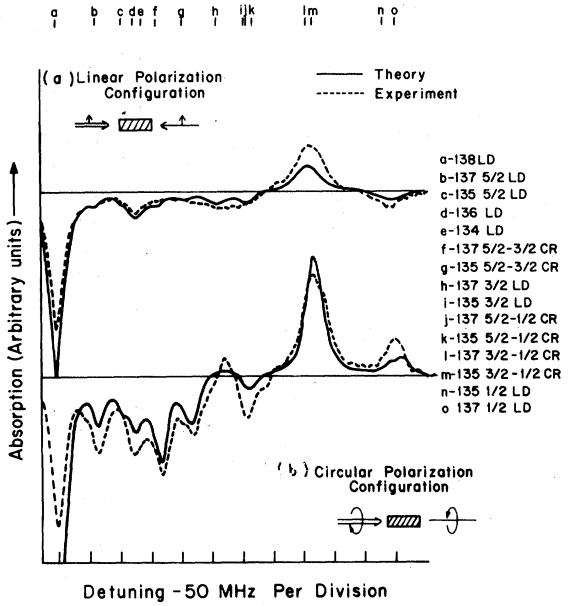

FIG. 6. Observed probe resonances (dotted curves), and theoretical fits (solid curves). The latter are computed using $I/I_s = 0.26$ and $T = 3$ μsec. The odd isotope hyperfine resonances are specified by their upper-level F values. $F_{\text{lower}} = \frac{3}{2}$ in all cases. CR refers to crossover resonances. (a) Probe and saturating beams have the same linear polarizations. (b) Probe and saturating beams have opposite circular polarizations.

of the probe and saturating beams (2.5 MHz); (the angle between probe and saturating beams was 4 mrad).

B. Comparison with theory

In order to obtain quantitative theoretical predictions for comparison with the experiments, expressions for α_p applicable to the barium resonance transitions were derived. The even isotope transitions are essentially nondegenerate (because of selection rules for a given polarization configuration), and so calculation of their Lamb dips is straightforward. The odd isotopes, however, have hyperfine structure, and so computation of the Lamb dips at the hyperfine transitions and crossover resonances between coupled hyperfine transitions is more complex because of the M degeneracies of the hyperfine levels.

The procedure[22] is the same as in Sec. II. For a given hyperfine transition, coupled rate equations for the populations of the M sublevels, as influenced by the saturating beam,[23] are written down [compare Eqs. (10)]. Radiative decay at both the pump transition and the 1.5-μm branching transition is included. (As discussed in Sec. II C 1, decay via the branching transition can give rise to D-state pileup and influence the width and depth of the saturation resonances.) The matrix elements and partial decay rates are computed using the appropriate Clebsch-Gordan coefficients. As in Eqs. (14), the steady-state solutions to the coupled rate equations are obtained. In analogy with Eqs. (24), (28), and (33), the probe gain coefficient for a given M component of a hyperfine transition is obtained by multiplying the appropriate population difference by the relevant probe absorption cross section (which again depends on the polarization state of the probe field). The Doppler velocity integrations can be conveniently performed using partial fraction decomposition and contour integration. Finally, the net probe gain coefficient (α_p) for a given hyperfine line is obtained by summing together the α_p's for each degenerate hyperfine M transition. A sample calculation is given in the Appendix.

The final results are tabulated in Tables II–VII.

TABLE II. Definitions of constants used in Tables III–VII.

$$\alpha_p(\Omega, I, T) = -N\sigma_D(0)\sum_{i=1}^{15} f_i g_i \left(1 - \sum_j \Theta_{ij} M(I_{ij}, \Delta_i)\right) \exp\left[-\left(\frac{\Delta_i}{ku}\right)^2\right]$$

N = barium density

$\sigma_D(0) = \sigma_0(\gamma\sqrt{\pi}/2ku) \simeq 4.5\times10^{-11}$ cm^2

$\sigma_0 = 3\lambda^2/2\pi = 1.5\times10^{-9}$ cm^2

$\gamma = 1/\tau + 2/T$, $\tau = 8.36$ nsec

$\gamma' = {}^1P_1 - {}^1D_2$ partial decay rate $= (0.2\ \mu\text{sec})^{-1}$

For a given barium isotope (Table III)

f_i = isotopic abundance

g_i = hyperfine level statistical weight

ω_i = 553-nm atomic center frequency $= \delta_i + \omega_{138}$

$\Delta_i = \Omega - \omega_i$

$$M(I_{ij}, \Delta_i) = \frac{S_{ij}(w_{ij}/2)^2}{\Delta_i^2 + (w_{ij}/2)^2}$$

$$S_{ij} = \frac{I/I_{ij}}{Q_{ij}(1+Q_{ij})}, \quad w_{ij} = \tfrac{1}{2}\gamma(1+Q_{ij}), \quad Q_{ij} = (1+I/I_{ij})^{1/2}$$

$$I_{ij} = 2I_s(\tau/T)J_{ij}, \quad I_s = \hbar\omega/2\sigma_0\tau = 14\ \text{mW/cm}^2$$

$$\Phi(I_{ij}, \Delta_i) = \tfrac{1}{2} S_{ij}/Q_{ij} + 4M(I_{ij}, \Delta_i)$$

The tables use the following constants:

$$u = \left(1 - \frac{9}{5}\gamma'\tau\frac{(2+\gamma' T)}{(\gamma' T)}\right)^{1/2}, \quad v = \left(1 - \frac{112}{15}\gamma'\tau\frac{(2+\gamma' T)}{(\gamma' T)}\right)^{1/2}$$

$$a = \frac{23}{10}\left(1 + \frac{13/5}{1-40\tau/T}\right), \quad b = \frac{7}{2}\left(1 + \frac{25}{17-200\tau/T}\right), \quad c = -\frac{525}{188}\left(1 + \frac{7/5}{1-10\tau/T}\right)$$

$$d = \frac{(23-100\tau/T) - 3(3a+7b+8c)/4}{4(1+50\tau/T)} = \frac{100 - 3(3a+7b+8c)}{16(1+50\tau/T)} - \frac{1}{2}$$

TABLE III. Isotopic abundance, statistical weights, and isotopic shift from 138 (see Table II for definitions).

Component [a]	i	f_i [b]	g_i	δ_i (MHz) [c]
Lamb dips				
138	1	0.72	1	0
136	2	0.08	1	125
134	3	0.024	1	140
137 ($\frac{1}{2}$)	4	0.11	$\frac{1}{6}$	555
137 ($\frac{3}{2}$)	5	0.11	$\frac{1}{3}$	260
137 ($\frac{5}{2}$)	6	0.11	$\frac{1}{2}$	65
135 ($\frac{1}{2}$)	7	0.066	$\frac{1}{6}$	535
135 ($\frac{3}{2}$)	8	0.066	$\frac{1}{3}$	305
135 ($\frac{5}{2}$)	9	0.066	$\frac{1}{2}$	105
Crossover resonances				
137 ($\frac{1}{2}$-$\frac{3}{2}$)	10	0.11	$\frac{1}{2}$	407.5
137 ($\frac{1}{2}$-$\frac{5}{2}$)	11	0.11	$\frac{2}{3}$	310
137 ($\frac{3}{2}$-$\frac{5}{2}$)	12	0.11	$\frac{5}{6}$	162.5
135 ($\frac{1}{2}$-$\frac{3}{2}$)	13	0.066	$\frac{1}{2}$	420
135 ($\frac{1}{2}$-$\frac{5}{2}$)	14	0.066	$\frac{2}{3}$	320
135 ($\frac{3}{2}$-$\frac{5}{2}$)	15	0.066	$\frac{5}{6}$	205

[a] The numbers in parentheses refer to the upper F values ($F_{\text{lower}}=\frac{3}{2}$).

[b] C. M. Lederer, J. M. Hollander, I. Perlman, *Table of Isotopes*, 6th ed. (Wiley, New York, 1967), pp. 76–77.

[c] D. H. Tuan, Proc. R. Soc. London, Ser. A 280, 323 (1964).

The line shapes computed from Tables II–VII are plotted as solid lines in Fig. 6. The saturation parameter used is $I/I_s = 0.26$, corresponding to our experimental conditions of a saturating beam power of 45 μW and a beam intensity diameter (e^{-1} points) of $D = 1.25$ mm. For the even barium isotopes, σ_0 of Eq. (7) is 1.5×10^{-9} cm^2, so that I_s of Eq. (4) is 14 mW/cm^2. In our experiments, T is determined by transit time. The value of $T = 3$ μsec was estimated from $T \simeq D/u\sqrt{2}$ with $D/\sqrt{2}$ the $1/e$ diameter of the E-field cross section and $u = 3.0 \times 10^4$ the rms atomic velocity. The computed curves are not sensitive to the value of T used. Variations over the range of 1–6 μsec produced only slight changes. Inspection of Tables II–VII reveals that this is so because in this region of parameters the effective saturation parameter is close to unity. As can be seen, the fit is satisfactory. The positions of the saturation resonances, their relative magnitudes, and the sign changes which occur when the linear pump-linear probe polarization configuration is changed to circular pump-circular probe are all in good agreement with the predictions.

IV. CONCLUDING REMARKS

The overall agreement of the barium experiments with the theoretical predictions confirms the important role that optical pumping can play in the laser saturation process in atomic resonance transitions. It would also be of interest to perform detailed studies of line shapes of the optical-pumping resonances as influenced by transit time, buffer gas pressure, and other nonradiative relaxation processes. Such studies were precluded in our experiments due to the large number of closely spaced saturation resonances in naturally occurring barium. Experiments along these lines could be performed using isotopically enriched ^{137}Ba or another sample gas with simpler structure.

In the above discussions nonradiative relaxation processes have been treated in a generalized way. At moderate pressures ($\geq$mtorr) and/or large laser beam diameters, the nonradiative decay time T will be determined by collisional relaxation processes. If the laser field is not sufficiently monochromatic, T will also be influenced by the finite laser bandwidth. At sufficiently low pressures (and for a laser field of sufficiently narrow bandwidth) T will be determined by the atomic transit time. In this case the terms in T in the rate equations (10) should be considered as an approximate way of including transit time effects. A detailed calculation along the lines of Ref. 24 has recently been completed. The results, which confirm the present calculations, will be reported separately.[25]

The phenomenon described here should also be useful in exploring the effects of buffer gases, wall collisions, etc., on destroying atomic nuclear orientation. The influence of M-changing and velocity-changing collisions, diffusion processes, and radiative transfer can all be studied. Laser optical-pumping saturation effects should also manifest themselves in coherent laser transients[26] and in laser saturation studies in the time-delayed mode.[27]

TABLE IV. Θ_{ij}—linear polarization (see Table II for definitions).

i \ j	1	2	3	4
1	1	0	0	0
2	1	0	0	0
3	1	0	0	0
4	1	0	0	0
5	$\frac{1}{2}+\frac{7}{50u}$	$\frac{1}{2}-\frac{7}{50u}$	0	0
6	$\frac{1}{2}-\frac{31}{50v}$	$\frac{1}{2}+\frac{31}{50v}$	0	0
7	1	0	0	0
8	$\frac{1}{2}+\frac{7}{50u}$	$\frac{1}{2}-\frac{7}{50u}$	0	0
9	$\frac{1}{2}-\frac{31}{50v}$	$\frac{1}{2}+\frac{31}{50v}$	0	0
10	$-\frac{8}{15}$	$\frac{13-5u}{30u}\left(\frac{\tau}{2T(1+u)}-1\right)$	$\frac{13+5u}{-30u}\left(\frac{\tau}{2T(1-u)}-1\right)$	0
11	$\frac{3}{20}$	$\frac{11-5v}{40v}\left(\frac{8\tau}{2T(1+v)}-1\right)$	$\frac{11+5v}{-40v}\left(\frac{8\tau}{2T(1-v)}-1\right)$	0
12	$\frac{-3}{50u}\left(\frac{(3+21u)\tau}{2T(1+u)}+\frac{33-25u}{5}\right)$	$\frac{3}{50u}\ \frac{(3-21u)\tau}{2T(1-u)}+\frac{33+25u}{5}$	$\frac{1}{125v}\left(\frac{(20-140v)\tau}{2T(1+v)}-(1-25v)\right)$	$\frac{-1}{125v}\left(\frac{(20+140v)\tau}{2T(1-v)}-(1+25v)\right)$
13	$-\frac{8}{15}$	$\frac{13-5u}{30u}\left(\frac{\tau}{2T(1+u)}-1\right)$	$\frac{13+5u}{-30u}\left(\frac{\tau}{2T(1-u)}-1\right)$	0
14	$\frac{3}{20}$	$\frac{11-5v}{40v}\left(\frac{8\tau}{2T(1+v)}-1\right)$	$\frac{11+5v}{-40v}\left(\frac{8\tau}{2T(1-v)}-1\right)$	0
15	$\frac{-3}{50u}\left(\frac{(3+21u)\tau}{2T(1+u)}+\frac{33-25u}{5}\right)\frac{3}{vu}$	$\left(\frac{(3-21u)\tau}{2T(1-u)}+\frac{33+25u}{5}\right)$	$\frac{1}{125v}\left(\frac{(20-140v)\tau}{2T(1+v)}-(1-25v)\right)$	$\frac{-1}{125v}\left(\frac{(20+140v)\tau}{2T(1-v)}-(1+25v)\right)$

TABLE V. J_{ij}—linear polarization (see Table II for definitions).

i \ j	1	2	3	4
1	$\frac{T/\tau+1}{2+\gamma' T}$			
2	$\frac{T/\tau+1}{2+\gamma' T}$			
3	$\frac{T/\tau+1}{2+\gamma' T}$			
4	6			
5	$\frac{15}{2(1+u)}$	$\frac{15}{2(1-u)}$		
6	$\frac{20}{3(1+v)}$	$\frac{20}{3(1-v)}$		
7	6			
8	$\frac{15}{2(1+u)}$	$\frac{15}{2(1-u)}$		
9	$\frac{20}{3(1+v)}$	$\frac{20}{3(1-v)}$		
10	6	$\frac{15}{2(1+u)}$	$\frac{15}{2(1-u)}$	
11	6	$\frac{20}{3(1+v)}$	$\frac{20}{3(1-v)}$	
12	$\frac{15}{2(1+u)}$	$\frac{15}{2(1-u)}$	$\frac{20}{3(1+v)}$	$\frac{20}{3(1-v)}$
13	6	$\frac{15}{2(1+u)}$	$\frac{15}{2(1-u)}$	
14	6	$\frac{20}{3(1+v)}$	$\frac{20}{3(1-v)}$	
15	$\frac{15}{2(1+u)}$	$\frac{15}{2(1-u)}$	$\frac{20}{3(1+v)}$	$\frac{20}{3(1-v)}$

ACKNOWLEDGMENTS

Discussions with and technical assistance from Martin Deutsch, Jeff Hunt, Ali Javan, Emily Kintzer, Thomas Kühl, Larry Lembo, and Bill Ryan are gratefully acknowledged. The work of P.G.P., M.M.B., D.D.H., and M.S.F. was supported in part by D.O.E. under Contract No. ER-78-S-02-4629, through MIT's Laboratory for Nuclear Science.

APPENDIX

As an example of the procedure used to obtain the theoretical expression for the barium saturation spectrum, $\alpha_p(\Omega, I, T)$ of Tables II–VII, we give here a sample calculation for the Lamb dip at the ${}^1S_0(F=\frac{3}{2}\rightarrow{}^1P_1(F=\frac{1}{2})$ transition when both saturating and probe beams are linearly polarized in the same direction. This particular calculation describes two components in the observed saturation spectrum, one for ^{137}Ba and one for ^{135}Ba.

The relevant energy levels and transitions are shown in Fig. 7. Since both lasers have the same linear polarization they induce transitions between two pairs of M_F sublevels, $M_F=\pm\frac{1}{2}\rightarrow M_F=\pm\frac{1}{2}$, i.e., the $d\rightarrow a$ and $e\rightarrow b$ transitions.

The expression for α_p, the probe gain coefficient, is a straightforward generalization of Eq. (24):

$$\alpha_p=\int_{-\infty}^{\infty}[(n_a-n_d)\sigma_{ad}(-x)+(n_b-n_e)\sigma_{be}(-x)]\,dx\,, \tag{A1}$$

where [cf. Eq. (5)]

$$\sigma_{ad}(x)=\sigma_{be}(x)=\frac{\sigma_0}{3}\frac{(\gamma/2)^2}{(\Delta_i-x)^2+(\gamma/2)^2}\,, \tag{A2}$$

with γ, σ_0, and Δ_i as in Tables II–VII, with $i=4$ (^{137}Ba Lamb dip) or $i=7$ (^{135}Ba Lamb dip). The rate equations for the n_j's are [cf. Eqs. (10)]

$$\dot{n}_a=(n_d-n_a)[\sigma_{ad}(x)I/\hbar\omega]-n_a(\Gamma+\gamma'+1/T)\,, \tag{A3}$$

$$\dot{n}_b=(n_e-n_b)[\sigma_{be}(x)I/\hbar\omega]-n_b(\Gamma+\gamma'+1/T)\,, \tag{A4}$$

$$\dot{n}_c=n_a\Gamma/2+(n_c^0-n_c)/T\,, \tag{A5}$$

$$\dot{n}_d=-(n_d-n_a)[\sigma_{ad}(x)I/\hbar\omega]+n_a\Gamma/3+n_6\Gamma/6+(n_d^0-n_d)/T\,, \tag{A6}$$

$$\dot{n}_e=-(n_e-n_b)[\sigma_{ad}(x)I/\hbar\omega]+n_b\Gamma/3+n_a\Gamma/6+(n_e^0-n_e)/T\,, \tag{A7}$$

$$\dot{n}_f=n_6\Gamma/2+(n_f^0-n_f)/T\,, \tag{A8}$$

where

$$n_c^0=n_d^0=n_e^0=n_f^0=f_iN/4G(x)\,, \tag{A9}$$

$$G(x)=(1/ku\sqrt{\pi})\exp[-(kv/ku)^2]\,, \tag{A10}$$

with f_i and N defined in Table II. (See the discussion following Eqs. (10) for further details.) The steady-state solutions of these equations are [cf. Eqs. (14)]

$$n_a=n_b=\frac{N}{4}f_iG(x)\frac{I}{I+I'}\left(\frac{2}{2+(\gamma+\gamma')T}\right)L_i(x)\,, \tag{A11}$$

$$n_d=n_e=\frac{N}{4}f_iG(x)\left[1-\frac{I}{I+I'}\left(\frac{(\gamma+\gamma')T}{2+(\gamma+\gamma')T}\right)L_i(x)\right], \tag{A12}$$

$$n_c=n_f=\frac{N}{4}f_iG(x)\left[1+\frac{I}{I+I'}\left(\frac{\Gamma T}{2+(\gamma+\gamma')T}\right)L_i(x)\right], \tag{A13}$$

where

TABLE VI. Θ_{ij}—circular polarization (see Table II for definitions).

i \ j	1	2	3	5	6	7
1	$\frac{2+\gamma' T}{2+\gamma' T}$	0	0	0	0	0
2	$\frac{1+\gamma' T}{2+\gamma' T}$	0	0	0	0	0
3	$\frac{1+\gamma' T}{2+\gamma' T}$	0	0	0	0	0
4	$-\left(\frac{11}{8}-\frac{9\tau}{4T}\right)$	$-\left(\frac{-3}{8}+\frac{\tau}{4T}\right)$	0	0	0	0
5	$-\left(\frac{17}{15}-\frac{3\tau}{T}\right)$	$-\left(\frac{-4}{5}+\frac{36\tau}{7T}\right)$	$\left(\frac{2}{15}-\frac{8\tau}{9T}\right)\Phi(I_{5,3};\Delta_5)$	0	0	0
6	$-\left(\frac{a}{20}+\frac{289\tau}{180T}-\frac{77}{100}\right)$	$-\left(\frac{b}{20}-\frac{3}{5}+\frac{41\tau}{28T}\right)$	$-\left(\frac{c}{20}+\frac{21}{50}-\frac{21\tau}{20T}\right)$	$-\frac{d}{20}$	0	0
7	$-\left(\frac{11}{8}-\frac{9\tau}{4T}\right)$	$-\left(\frac{-3}{8}+\frac{\tau}{4T}\right)$	0	0	0	0
8	$-\left(\frac{17}{15}-\frac{3\tau}{T}\right)$	$-\left(\frac{-4}{5}+\frac{36\tau}{7T}\right)$	$\left(\frac{2}{15}-\frac{8\tau}{9T}\right)\Phi(I_{8,3};\Delta_8)$	0	0	0
9	$-\left(\frac{a}{20}+\frac{289\tau}{180T}-\frac{77}{100}\right)$	$-\left(\frac{b}{20}-\frac{3}{5}+\frac{41\tau}{28T}\right)$	$-\left(\frac{c}{20}+\frac{21}{50}-\frac{21\tau}{20T}\right)$	$-\frac{d}{20}$	0	0
10	$-\left(\frac{5}{6}+\frac{15\tau}{14T}\right)$	$\left(\frac{7}{18}+\frac{35\tau}{36T}\right)$	$-\left(\frac{11}{30}+\frac{6\tau}{25T}\right)$	$-\left(\frac{1}{10}-\frac{2\tau}{15T}\right)$	$-\left(\frac{2}{9}+\frac{5\tau}{27T}\right)\Phi(I_{10,5};\Delta_{10})$	0
11	$\frac{27}{160}-\frac{3\tau}{5T}$	$\frac{9}{160}-\frac{27\tau}{100T}$	$\frac{-3d}{16}$	$-\left(\frac{-1}{20}+\frac{\tau}{3T}+\frac{3a}{16}\right)$	$-\left(\frac{15\tau}{28T}-\frac{3}{16}+\frac{3b}{16}\right)$	$-\left(\frac{7}{40}-\frac{7\tau}{16T}+\frac{3c}{16}\right)$
12	$-\left(\frac{57}{250}-\frac{169\tau}{200T}+\frac{3c}{25}\right)$	$-\left(\frac{-9}{50}+\frac{27\tau}{70T}\right)$	$\left(\frac{2}{25}-\frac{\tau}{5T}\right)\Phi(I_{12,3};\Delta_{12})$	$-\frac{3d}{25}$	$-\left(\frac{-47}{250}+\frac{79\tau}{75T}+\frac{3a}{25}\right)$	$-\left(\frac{-27}{50}+\frac{51\tau}{35T}+\frac{3b}{25}\right)$
13	$-\left(\frac{5}{6}+\frac{15\tau}{14T}\right)$	$\frac{7}{18}+\frac{35\tau}{36T}$	$-\left(\frac{11}{30}+\frac{6\tau}{25T}\right)$	$-\left(\frac{1}{10}-\frac{2\tau}{15T}\right)$	$-\left(\frac{2}{9}+\frac{5\tau}{27T}\right)\Phi(I_{13,5};\Delta_{13})$	0
14	$-\left(\frac{3\tau}{5T}-\frac{27}{160}\right)$	$\frac{9}{160}-\frac{27\tau}{100T}$	$\frac{-3d}{16}$	$-\left(\frac{-1}{20}+\frac{\tau}{3T}+\frac{3a}{16}\right)$	$-\left(\frac{15\tau}{28T}-\frac{3}{16}+\frac{3b}{16}\right)$	$-\left(\frac{7}{40}-\frac{7\tau}{16T}+\frac{3c}{16}\right)$
15	$-\left(\frac{57}{250}-\frac{169\tau}{200T}+\frac{3c}{25}\right)$	$-\left(\frac{-9}{50}+\frac{27\tau}{70T}\right)$	$\left(\frac{2}{25}-\frac{\tau}{5T}\right)\Phi(I_{15,3};\Delta_{15})$	$-\frac{3d}{25}$	$-\left(\frac{-47}{250}+\frac{79\tau}{75T}+\frac{3a}{25}\right)$	$-\left(\frac{-27}{50}+\frac{51\tau}{35T}+\frac{3b}{25}\right)$

TABLE VII. J_{ij}—circular polarization (see Table II for definitions).

i \ j	1	2	3	4	5	6
1	$\frac{T/\tau+1}{2+\gamma' T}$					
2	$\frac{T/\tau+1}{2+\gamma' T}$					
3	$\frac{T/\tau+1}{2+\gamma' T}$					
4	$\frac{36}{5}$	4				
5	$\frac{25}{6}$	$\frac{225}{56}$	$\frac{25}{6}$			
6	$\frac{100}{9}$	$\frac{100}{21}$	$\frac{25}{6}$	$\frac{25}{1+50\tau/T}$		
7	$\frac{36}{5}$	4				
8	$\frac{25}{6}$	$\frac{225}{56}$	$\frac{25}{6}$			
9	$\frac{100}{9}$	$\frac{100}{21}$	$\frac{25}{6}$	$\frac{25}{1+50\tau/T}$		
10	$\frac{225}{56}$	$\frac{25}{6}$	$\frac{36}{5}$	4	$\frac{25}{6}$	
11	4	$\frac{36}{5}$	$\frac{25}{1+50\tau/T}$	$\frac{100}{9}$	$\frac{100}{21}$	$\frac{25}{6}$
12	$\frac{25}{6}$	$\frac{225}{56}$	$\frac{25}{6}$	$\frac{25}{1+50\tau/T}$	$\frac{100}{9}$	$\frac{100}{21}$
13	$\frac{225}{56}$	$\frac{25}{6}$	$\frac{36}{5}$	4	$\frac{25}{6}$	
14	4	$\frac{36}{5}$	$\frac{25}{1+50\tau/T}$	$\frac{100}{9}$	$\frac{100}{21}$	$\frac{25}{6}$
15	$\frac{25}{6}$	$\frac{225}{56}$	$\frac{25}{6}$	$\frac{25}{1+50\tau/T}$	$\frac{100}{9}$	$\frac{100}{21}$

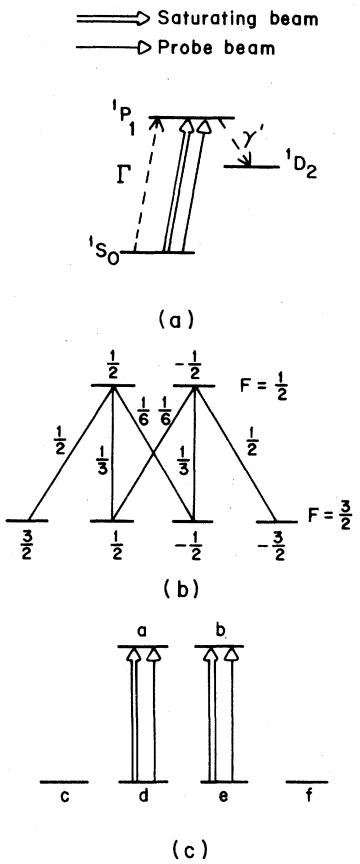

FIG. 7. Relevant energy levels and transitions for calculating $^1S_0(F=\frac{3}{2}) \rightarrow {}^1P_1(F=\frac{1}{2})$ Lamb dips. (a) Barium resonance transition showing D-state radiation decay. Γ and γ' are the spontaneous emission partial decay sites. Note that the branching ratio $\gamma'/(\Gamma+\gamma') = 0.04$. (b) Transitions among M_F sublevels. The spontaneous emission branching weights are indicated. (c) Probe and saturating beam transitions. Note that the linearly polarized laser fields both induce $\Delta M_F = 0$ transitions.

$$L_i(x) = \frac{(\gamma/2)^2(1+I/I')}{(\Delta_i - x)^2 + (\gamma/2)^2(1+I/I')} \tag{A14}$$

and

$$I' = 6\frac{\hbar\omega}{\sigma_0\tau}\left(\frac{1+\tau/T}{2+(\gamma+\gamma')T}\right). \tag{A15}$$

Substitution into Eq. (A1) then gives

$$\alpha_p = -\frac{Nf_i}{12}\int_{-\infty}^{\infty}\left(1 - \frac{I}{I+I'}L_i(x)\right)\sigma(-x)G(x)dx\,, \tag{A16}$$

which is similar to Eqs. (17) and (24) of the text. Integration gives

$$\alpha_p = -\tfrac{1}{6}N\sigma_D(0)f_i[1 - M(I', \Delta_i)]e^{-(\Delta_i/ku)^2}\,, \tag{A17}$$

with $M(I', \Delta_i)$ defined in Table II. Since $\gamma \gg \gamma'$ and $2/T$,

$$I' \simeq 6\hbar\omega/\sigma_0 T\,. \tag{A18}$$

This result appears as the $i=4$ (^{137}Ba) and $i=7$ (^{135}Ba) contributions to $\alpha_p(\Omega, I, T)$ of Table II. From Table III, $f_4 = 0.11$, $g_4 = \frac{1}{6}$, $\delta_4 = 555$ MHz, $f_7 = 0.066$, $g_7 = \frac{1}{6}$, $\delta_7 = 535$ MHz, where $\Delta_i = (\Omega - \omega_{138}) - \delta_i$(Table III). From the linear polarization entries of Table IV, the only two nonzero Θ_{ij}'s for $i=4$ and 7 are $\Theta_{41} = \Theta_{71} = 1$. From Table V $J_{41} = J_{71} = 1$, which gives $I_{41} = I_{71} = 12I_s\tau/T = I'$ of Eq. (A16). Hence, for $i=4$ and 7, $M(I_{i1}, \Delta_i) = M(I', \Delta_i)$.

[1]For reviews, see V. S. Letokhov and V. P. Chebotaev, in *Nonlinear Laser Spectroscopy*, edited by D. L. McAdam (Springer, Berlin, 1977), Vol. 4; M. S. Feld, in *Fundamental and Applied Laser Physics*, edited by M. S. Feld, N. A. Kurnit, and A. Javan (Wiley, New York, 1973), p. 369.

[2]See, for example, R. Bernheim, *Optical Pumping* (Benjamin, New York, 1965); W. Happer, Rev. Mod. Phys. 44, 169 (1972).

[3]M. Burns, P. Pappas, M. S. Feld, and D. E. Murnick, in *Hyperfine Interactions IV*, edited by R. S. Raghavan and D. E. Murnick (North-Holland, Amsterdam, 1978), p. 50.

[4]Preliminary results were presented in D. E. Murnick, M. Burns, D. Hinshelwood, P. Pappas, and M. S. Feld, *Digest of Technical Papers, Tenth International Quantum Electronics Conference*, IEEE Catalog No. 78, Chap. 1301-1-QEA, p. 649; and in D. E. Murnick, M. S. Feld, M. M. Burns, T. U. Kühl, and P. G. Pappas, in *Laser Spectroscopy IV*, edited by H. Walter and K. W. Rothe (Springer, Berlin, 1979), p. 195.

[5]D. E. Murnick, M. S. Feld, M. M. Burns, T. U. Kühl, and P. G. Pappas, Opt. Lett. 5, 79 (1980).

[6]W. Gawlik and G. W. Series, in *Laser Spectroscopy IV*, edited by H. Walter and K. W. Rothe (Springer, Berlin, 1979), p. 210.

[7]M. Pinard, C. G. Aminoff, F. Laloë, Phys. Rev. A 19, 2366 (1979).

[8]W. E. Lamb, Jr., Phys. Rev. A 134, 1429 (1964); and Ref. 1.

[9]J. Brossel, A. Kastler, and J. Winter, J. Phys. Radium 13, 668 (1952).

[10]H. R. Schlossberg and A. Javan, Phys. Rev. 150, 267 (1966).

[11]M. S. Feld and A. Javan, Phys. Rev. 177, 640 (1964); and Ref. 1.

[12]M. S. Feld, in *Frontiers in Laser Spectroscopy*, edited by R. Balian, S. Haroche, and S. Liberman (North-Holland, Amsterdam, 1977), Vol. 1, p. 203.

[13]For a Maxwellian velocity distribution of width ku: $G(x) = (1/ku\sqrt{\pi}) \exp[-(x/ku)^2]$, and so [cf. Eq. (19)] $\sigma_D(\Delta) = (4\pi^{3/2}\mu^2/\hbar u) \exp[-(\Delta/ku)^2]$.

[14]For simplicity, the present calculation neglects coherent Lamb-dip effects of the type discussed in Refs. 15 and 16. These treatments can be modified to include optical-pumping effects simply by changing the form of the relaxation terms in the diagonal density matrix elements to conform with Eqs. (10).

[15]S. Stenholm and W. E. Lamb, Jr., Phys. Rev. 181, 618 (1969); B. J. Feldman and M. S. Feld, Phys. Rev. A 1, 1375 (1970).

[16]E. V. Baklanov and V. P. Chebotaev, Zh. Eksp. Teor. Fiz. 60, 552 (1971) [Sov. Phys.-JETP 33, 300 (1971)]; S. Haroche and F. Hartmann, Phys. Rev. A 6, 1280 (1972).

[17]Note that at sufficiently low pressures $\Gamma_1 T$, hence the degree of optical pumping, can be experimentally varied by changing the diameter of the pump beam.

[18]T. Hänsch, I. S. Shahin, and A. Schawlow, Phys. Rev. Lett. 27, 707 (1971).

[19]H. Holt, Phys. Rev. Lett. 29, 1138 (1972).

[20]D. A. Jackson and D. H. Tuan, Proc. R. Soc. London Ser. A 280, 323 (1964).

[21]W. Rasmussen, R. Schieder, and H. Walther, Opt. Commun. 12, 315 (1974).

[22]D. D. Hinshelwood, S. B. thesis, MIT, 1978 (unpublished).

[23]As usual, the coupling of the pump field to the M sublevel depends on the polarization state of the pump field.

[24]S. G. Rautian and A. M. Shalagin, Zh. Eksp. Teor. Fiz. 58, 962 (1970) [Sov. Pnys.—JETP 31, 518 (1970)]; E. V. Baklanov, B. Ya. Dubetskii, V. M. Semibalamut, and E. A. Titov, Kvantovaya Elektron. 2, 2518 (1975) [Sov. J. Quantum Electron. 5, 1374 (1976)]; C. J. Bordé, J. L. Hall, C. V. Kunasz, and D. G. Hummer, Phys. Rev. A 14, 236 (1976); J. E. Thomas, M. J. Kelly, J.-P. Monchalin, N. A. Kurnit, and A. Javan, *ibid.* 15, 2356 (1977).

[25]J. E. Thomas and W. W. Quivers, Jr. (unpublished).

[26]See, for example, *Laser Spectroscopy III, Springer Series in Optical Sciences*, edited by J. L. Hall and J. L. Carlsten (Springer, Berlin, 1977).

[27]M. Ducloy, J. R. R. Leite, and M. S. Feld, Phys. Rev. A 17, 623 (1978).